ARCTIC RESPONSE TECHNOLOGY
OIL SPILL PREPAREDNESS

August, 2017

Nathan J. Lamie, Keran J. Claffey, Leonard J. Zabilansky, P.E.

EVALUATION OF INFRARED SENSORS AND VISIBLE SPECTRUM SENSORS TO DETECT OIL SPILLS ON ICE SURFACES.

ABSTRACT

Experiments were conducted December 2, 2016 through December 8, 2016 in the Geophysical Research Facility at the U.S. Army Cold Regions Research and Engineering Laboratory, Hanover, NH, USA to evaluate the applicability of infrared and visible spectrum imagers in the event of an oil spill on an ice surface in Arctic conditions. Once a safe load bearing sea ice sheet was established, a series of measurements were performed to evaluate the effectiveness of the imagers in differentiating between oil covered and clean ice surfaces. Images and data were recorded over a six day period. Two natural snow events occurred, offering a unique experimental opportunity. The angle of incidence of the imaging sensors was designed to simulate what would be seen from bridge deck mounted system. Results of non-intrusive, stand-off detection of surface oil spills in snow and ice conditions are discussed.

TABLE OF CONTENTS

LIST OF FIGURES

LIST OF TABLES

1 INTRODUCTION

Potential sources of Arctic oil spills in ice are producing oil wells, offshore exploration wells, marine pipelines, ships, and coastal fuel storage tanks. Remote Arctic villages often need to store significant volumes of heating oil, jet fuel and gasoline close to the shoreline due to long periods between resupply [1]. There is a possibility for oil spilled from a failed storage tank to run out onto the ice surface at the shore. A far less likely potential hazard involves the spring migration of oil to the ice surface following a subsea oil discharge [2], or oil deposited directly on top of the ice through loss of well control at the surface.

Oil exposed on the ice surface absorbs solar radiation and re-emits a portion of this radiation as thermal energy in the 8 to 14 μm spectral band. In a large-scale field experiment conducted during the winter of 1974/75, oil film temperatures were measured on melt pools in the spring as much as 10°C higher than the underlying water (the average temperature difference during periods of high radiation was 7°C [3]. Previous studies have investigated detection and relative thickness measurements of oil in the infrared band. Thickness measurements correlated to the re-radiation of thermal energy is poorly understood, but evidence indicates that both daytime and nighttime detection of exposed oil is possible if a significant temperature contrast is maintained. It should be noted that the necessary contrast between oil and water will vary with weather conditions (e.g. low cloud or fog) and in turn affect the possibility of oil detection in the infrared.

Previously mentioned studies focused on oil floating on water or ice melt pools or emulsified with sea water. This experiment investigated the infrared radiation from oil on an ice surface. Experimental results that differentiate ice, oil and snow with a fixed viewing geometry through several diurnal cycles are provided and discussed.

2 MATERIALS AND METHODS

This experiment was conducted in the Geophysical Research Facility (GRF) at the Cold Regions Research and Engineering Laboratory (CRREL) in Hanover, New Hampshire over the course of six days starting on December 2, 2016. The GRF is a 20 m x 7 m x 2.2 m deep outdoor basin capable of growing an ice sheet in cool temperate weather conditions by employing a removable refrigerated roof system. The ice sheet is grown in a quiescent environment that leads a smooth ice surface. Type T thermocouples were used to measure the ice sheet profile and water temperatures were logged hourly on a Campbell Scientific CR1000 data logger. GRF environmental data was recorded from the beginning of the formation of the ice sheet in mid-October, 2016 through the end of the experiment on December 8, 2016. The ice sheet was grown from a 27 parts per thousand (ppt) salt water solution. At the time of the experiment, the ice was 20 cm thick.

A 3 m x 3 m wooden frame was constructed using 1" x 4" (2.5 cm x 10 cm) lumber and was then frozen into the ice surface to create the target area of interest for this experiment. Eighty seven liters (23 gallons) of Alaska North Slope (ANS) crude oil were intentionally released into the target area, resulting in a nominal oil slick thickness of 1 cm. Oil temperature was periodically measured using a type K thermocouple connected to an Omega TrueRMS Supermeter.

A gantry trolley system constructed from steel I-beams spans the width of the GRF with a cross member that resides 3.2 m above the ice surface. A mounting plate for the infrared and visible spectrum sensors was mounted from the bottom of the steel cross member of the gantry trolley. The sensors were 3 m above the ice surface at a distance of 9 m to the south of the target area, creating an incidence angle of 30° down from horizontal.

2.1 Long Wave Infrared Camera

CRREL's ThermaCAM SC640 portable infrared camera was used to periodically record long wave imagery of the target area of interest. The ThermaCAM SC640 was designed by FLIR systems for scientific applications. The long wave camera functions in the 7.5 µm to 13 µm spectral range, and has high image quality of 640 x 480 pixels and on board data storage.

The long wave infrared data was recorded every 5 minutes throughout the experiment. The ThermaCAM Researcher software has measurement and analysis functions that were used to process this data for pixel by pixel comparisons throughout the course of the experiment.

2.2 Mid Wave Infrared Camera

CRREL's Silver 420M mid wave infrared camera was used to periodically record data in the 3 µm to 5 µm spectral range. The camera was developed by Cedip Infrared Systems for research and development applications. A laptop and external power supply are required to operate the camera. Data was recorded at 5 minute intervals using the ALTAIR software. The ALTAIR software was used to calibrate the camera as well as record and analyze the mid wave images.

2.3 FLIR Multi-Camera Pod

Shell Offshore Inc. contributed a FLIR MU Series Ultra Long-Range Multi-Sensor Thermal Night Vision System, model MC-602CLW, which is a multi-camera system containing a long wave, mid wave, visible, and low light visible cameras. The FLIR MU Series is a monitoring system with long range zoom and active gyro-stabilization designed for the maritime industry.

The MU series does not have on board image recording capabilities. Traditionally, the system displays a selected live image from one of its four cameras. It has picture-in-picture capability that allows display of a second camera with reduced resolution. The system was powered using an external power supply.

Through the network connection of the FLIR Pod, two live images of selected cameras were displayed on a laptop PC. Initially, the long wave and mid wave cameras were selected. The long wave and low light visible camera were selected for the majority of the experiment. VLC software was used to record screen captures of the live images and saved to disc. Periodic images were saved every minute.

Sensor specifications are described in Table 1.

Imager	Spectral Range	Resolution	Lens (width x height)
FLIR SC640	7.5 - 13 µm	640 x 480 pixels	45° x 34° FOV
Silver 420M	3.6 - 5 µm	320 x 256 pixels	38° x 30.4° FOV
MC-602CLW - Long Wave	7.5 - 13.5 µm	640 x 480 pixels	32° x 24° FOV
MC-602CLW - Mid Wave	3 - 5 µm	640 x 512 pixels	28° x 22.4° FOV
MC-602CLW - Visible Color	350 to 700 nm	550 TV Lines	56° FOV
MC-602CLW - Low Light b/w	350 to 1000 nm	570 TV Lines	41° FOV

Table 1: Imager Specifications.

3 SENSOR PERFORMANCE

Incoming solar energy was recorded with Eppley Laboratory radiometers located near the GRF test site. A Precision Infrared Radiometer (PIR) recorded incoming short wave solar irradiance in the spectral range of 4 to 50 µm with a field of view near 180°. An Eppley Precision Spectral Pyranometer (PSP) recorded incoming long wave solar irradiance in the spectral range of 0.295 to 2.8 µm. Data was sampled once a minute by a Campbell Scientific CR1000 data logger. The sampled data was averaged and recorded once every 15 minutes. Air temperature, relative humidity, and barometric pressure were also recorded.

Figure 1 shows the response of the PSP and PIR instruments over the course of the experiment. PSP and PIR data can be considered "light" and "heat" from the sun, respectively. The PSP data (red) depicts this with the highest response (most light) during mid-day and near zero at night. Minimal PSP response can be seen on December 5 and December 7, which were two overcast days with frequent snow events. This radiometer data gives insight to the spectral response of the three sensors being evaluated.

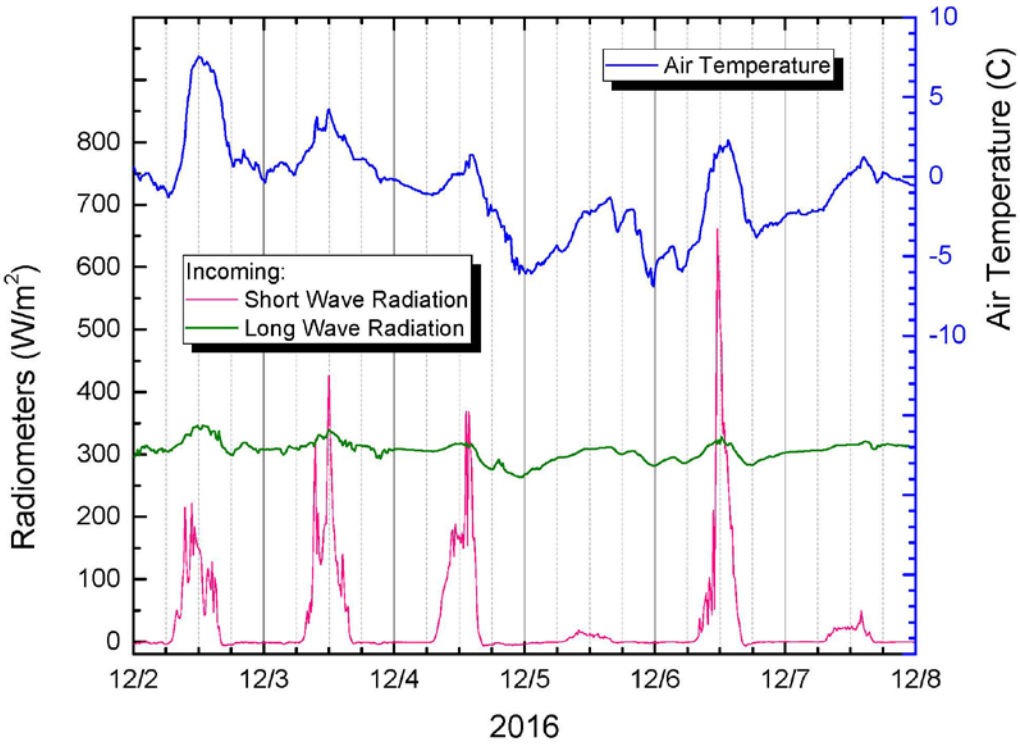

Figure 1 Incoming solar irradiance measured by Eppley Laboratories PSP (short wave) and PIR (long wave) radiometers and recorded air temperature.

The physical temperature of the spilled oil was recorded periodically with a handheld Omega TrueRMS Supermeter and was typically the same magnitude as the ice surface temperature sensor that was measured by a type T thermocouple and recorded hourly by a Campbell Scientific

CR1000 data logger. Recall that the infrared cameras respond to the re-emitted thermal energy [4] more than the physical temperature of the target.

Figure 2 shows a sample image of the target area of interest recorded by the FLIR S60 long wave camera. The two boxed areas are portions of the image that are further analyzed. Area of Interest 1 (AoI 1) is a sample area of exposed ice. Area of Interest 2 (AoI 2) is a sample of 1cm of ANS crude oil spilled on the ice surface.

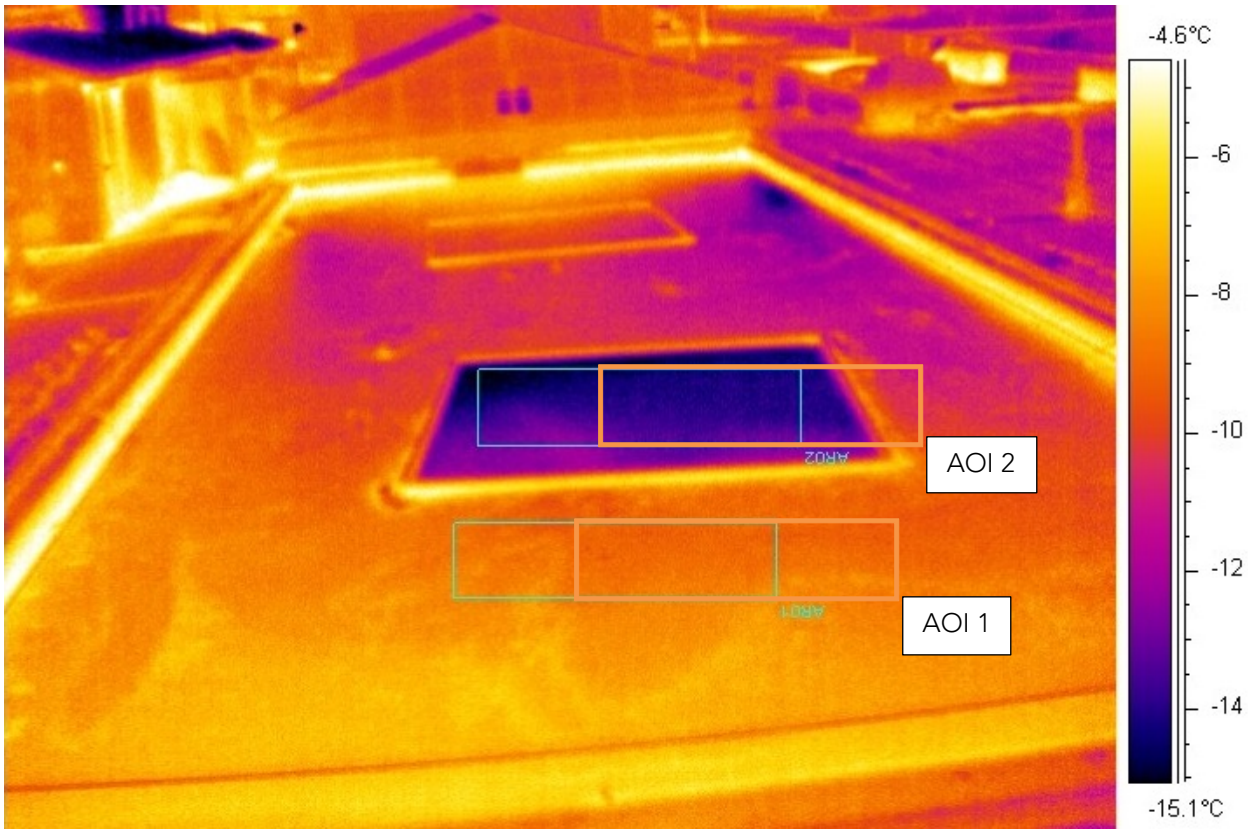

Figure 2 FLIR SC640 long wave camera image of experimental scene.

The ThermaCAM Researcher software was used to compile all of these images. Each pixel of the 640 x 480 pixel scene has an associated radiative temperature. To analyze the data, areas of interest were separately boxed and all radiating temperatures within each box were averaged. This resulted in two data points; 1) An average temperature for an exposed ice cover (AoI 1) and 2) An exposed oil slick on ice (AoI 2). This data was collected in five minute intervals. The mid wave data was processed with the same approach using the Cedip ALTAIR software.

The FLIR MU Series Pod was not designed as a scientific research tool. With two display channels available, the long wave and mid wave cameras were monitored and recorded using the freeware VLC screen capture software. Soon after being exposed to the outdoor environment the mid wave camera on the FLIR Pod experienced malfunctions with increasing frequency. It is suspected that the cooling mechanism for the mid wave camera could not tolerate the cold environment. Functionality of the mid wave camera occurred once returned to the lab environment and allowed time to warm to room temperature.

It was decided that camera recordings from that point on would be limited to the long wave infrared camera and the low light visible camera. Intermittent connectivity errors did occur. It is unclear whether the cause was within the FLIR pod or from the additional VLC software. Limited analysis was possible with the FLIR Pod long wave camera. Images from the FLIR Pod were compared to images collected at the same time with the FLIR SC640 camera. The two systems operate at nearly the same spectral range (see Table 1) and operated generally within a similar range of environmental parameters. The lens FLIR SC640 has a field of view 40.6% larger than the FLIR Pod. The manual zoom of the FLIR Pod was adjusted to capture a similar scene as the FLIR SC640.

4 RESULTS

The results for each sensor are given in the sections below. The experiment occurred over several days in early December of 2016. The sun azimuth was 210.5° with an elevation of 19.5°. The sun declination was 21°52′ south. Air temperatures cycled above and below freezing over the course of the experiment. Two snow events occurred; one on December 5th and the other on December 6th.

4.1 FLIR Pod Low Light Visible Spectrum Camera

The low light camera recorded imagery from December 3 to December 5. Figure 3 shows a sample image recorded at 01:00 AM on December 5.

Figure 3 Sample image from FLIR Pod MU Series low light visible spectrum camera.

The low light camera functioned consistently aside from network connection interrupts. Clear contrast between the ice surface and oil surface is evident.

4.2 FLIR Pod Long Wave Infrared Camera

As indicated above, long wave imagery from the FLIR Pod is comparable to the FLIR SC640. As evidence, compare Figure 4, a long wave image from the FLIR Pod, with Figure 2, from the FLIR S60.

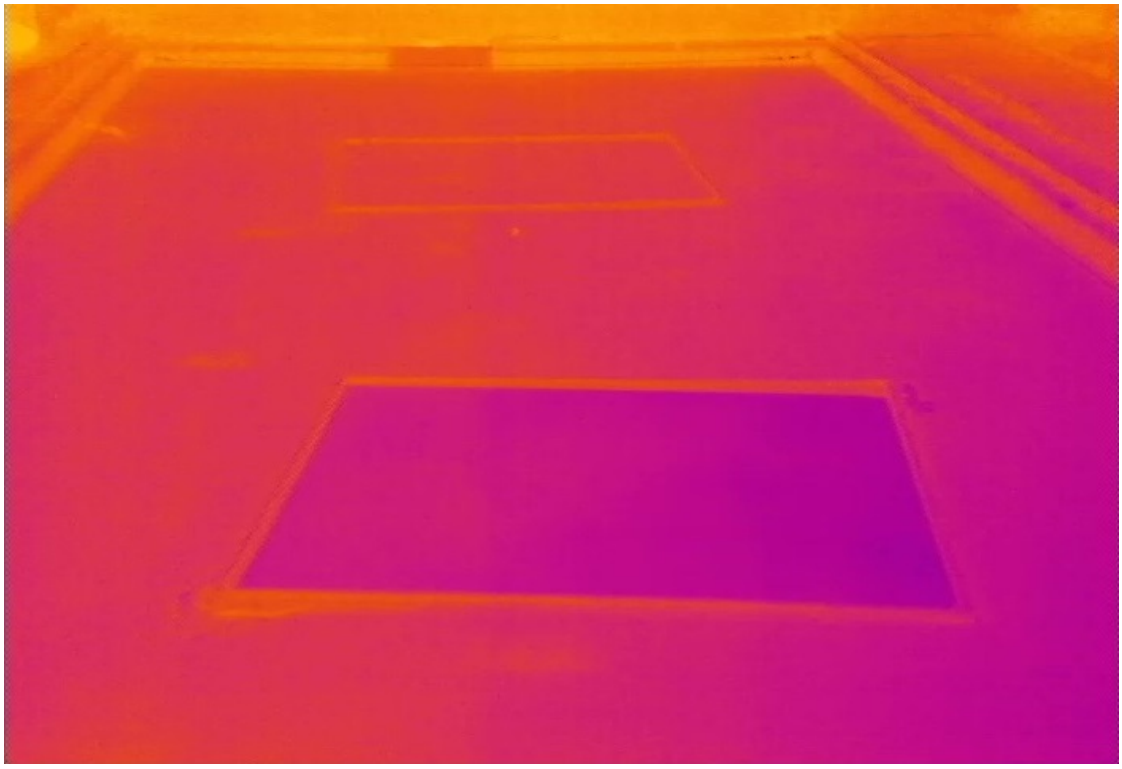

Figure 4 Sample image from FLIR MU Series long wave infrared camera.

An important asset of the FLIR Pod is the powerful optical zoom active gyro stabilization. Comparing the contrast and resolution of the image in Figure 4 to that of the FLIR SC640 (Figure 2) shows a better result with the FLIR SC640. There are two reasons for this. First, the seemingly poorer resolution is mostly due to the wide angle lens used with the FLIR SC640. The lens of the FLIR Pod long wave camera has a smaller field of view compared to the FLIR SC640 (see Table 1.). The image from the FLIR Pod is zoomed out to cover the same area of interest as the FLIR SC640, resulting in what seems to be a poorer resolution because each pixel is covering a larger physical area then the FLIR SC640. Second, the FLIR Pod uses an automatic gain control to set the maximum and minimum temperatures in the scene. The FLIR SC640 has an adjustable temperature window, so the max and mid temperatures can be more finely controlled, resulting in better image contrast.

In some cases the FLIR Pod seemed to have difficulty recalibrating. As temperatures changed over the day, an image would completely wash out (lose contrast), with surrounding structures barely visible. In some cases the oil and ice were undistinguishable due to weather effects like overcast skies. The oil was unidentifiable after the first snowfall. Contrast between features of the scene then became insufficient to provide a clear disparity.

4.3 FLIR S60 Long Wave Infrared Camera

Figure 5 is a comparison plot of the oil covered area and the exposed ice areas. The oil covered area is more reactive to irradiation events. When the temperatures rise there is an evident separation of radiative temperature readings. This occurs again notably when the temperature drops sharply. The radiative temperature of the object in the image is not the same parameter as

the physical temperature of the object. The long wave radiation detected by the imager is correlated to the emissivity along with the physical temperature of the object.

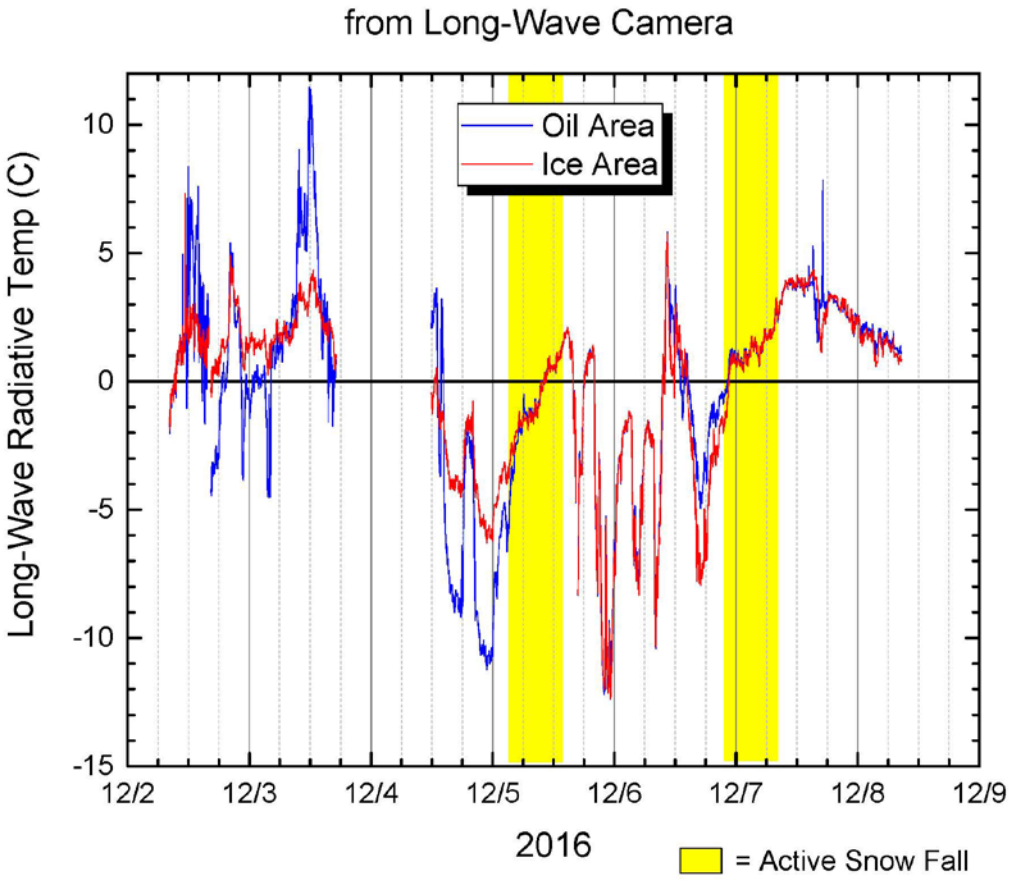

Figure 5 Plot of FLIR S60 camera data comparing an oil covered surface to an exposed ice covered surface.

There are two critical times of day when these large temperature differences occur. The first critical time corresponds with the peak of solar loading beginning around 10:00. This can be compared to the incoming solar irradiation recorded in Figure 1. Just after sunrise the black oil surface begins to re-radiate the solar heat much more effectively than the bare white ice surface. The second critical time is right after sundown (around 16:30 in early December). The drastic drop in radiative temperature occurs because the black surface is radiating the stored energy but no longer radiates the reflected solar energy.

The direct surface temperature differences between the oiled area and clean ice area are plotted in Figure 6 and compared with the air temperature. This is an alternate way to view the dataset. Note the snow events in Figure 5 and 6. In Figure 6 it is interesting to note that before the second snow event, there begins to be a difference in radiative temperature between the two areas of interest. Both surfaces are still covered with naturally fallen snow, yet shortly before the second snowfall, there is evidence of a detection. This indicates that some solar energy is penetrating the snow. This action repeats about 8 hours after the second snow fall as well.

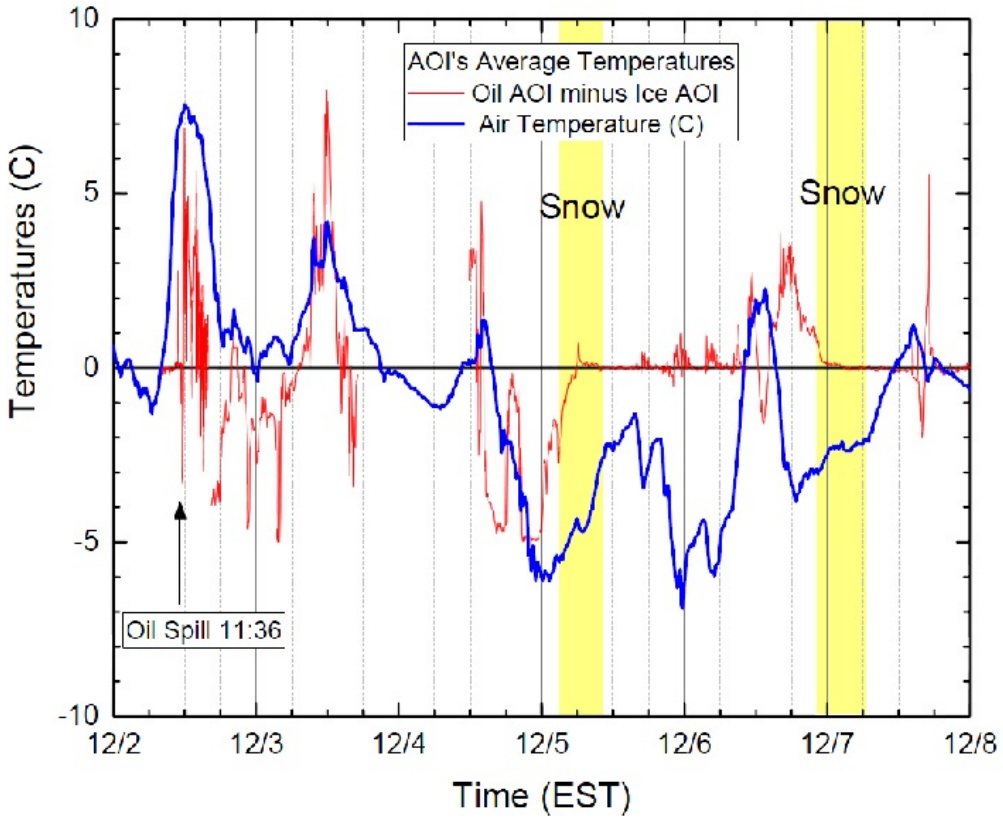

Figure 6 Temperature difference between oil covered surface and an exposed ice covered surface recorded with the FLIR S60 compared to the air temperature.

4.4 Cedip Silver 420M Mid Wave Infrared Camera

Similar analysis was conducted with the mid wave camera data. Figures 7 is a comparison of the mid wave radiative temperatures of the oil area and exposed ice area. Mirroring the results of the long wave camera, the oil surface in the mid wave spectrum reacts slightly more drastically than the natural ice surface. The oiled vs. clean ice temperature differences recorded at times of maximum solar radiation are in the same order as the differences between oil films on melt pools and the underlying water measured in field experiments [3].

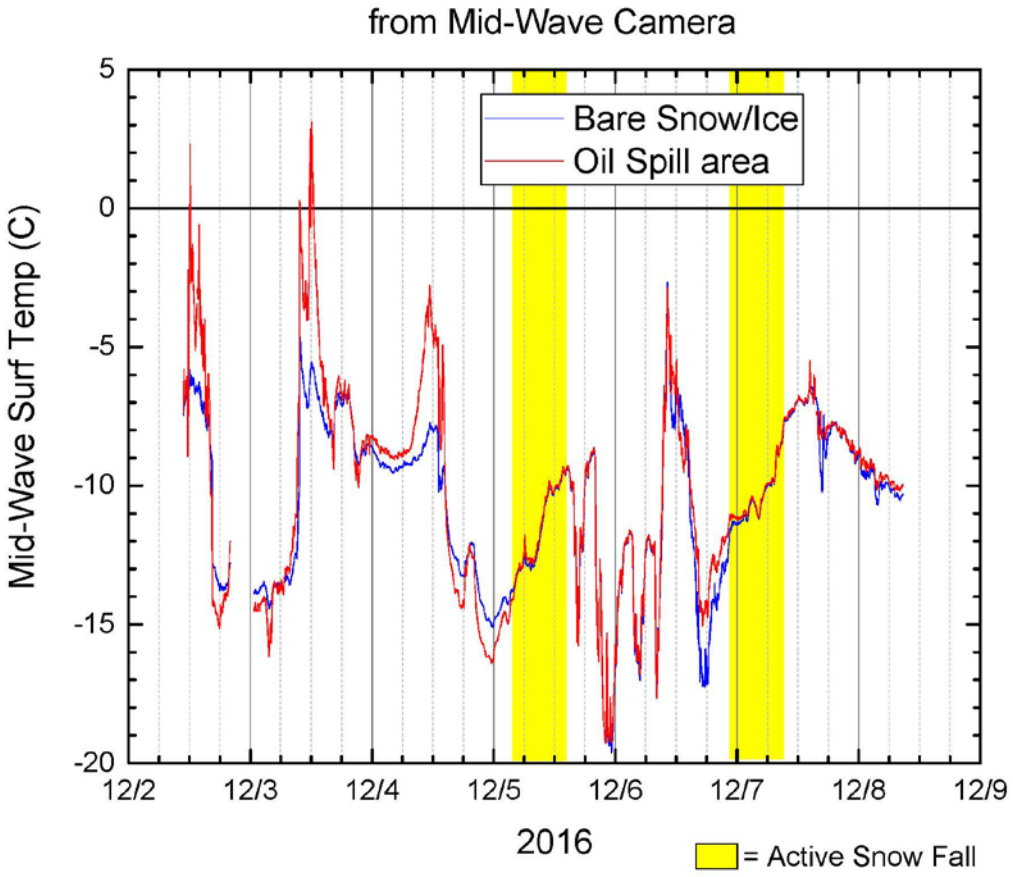

Figure 7 Plot of Cedip Silver 420M camera data comparing an oil covered surface to an exposed ice covered surface.

Figure 8 compares mid wave camera results with the long wave. The data tracks one another with one exception. The long wave data is more reactive when the sun goes down. When the sun is no longer visible and temperatures drop the long wave data drops drastically and stays well below the mid wave equivalent.

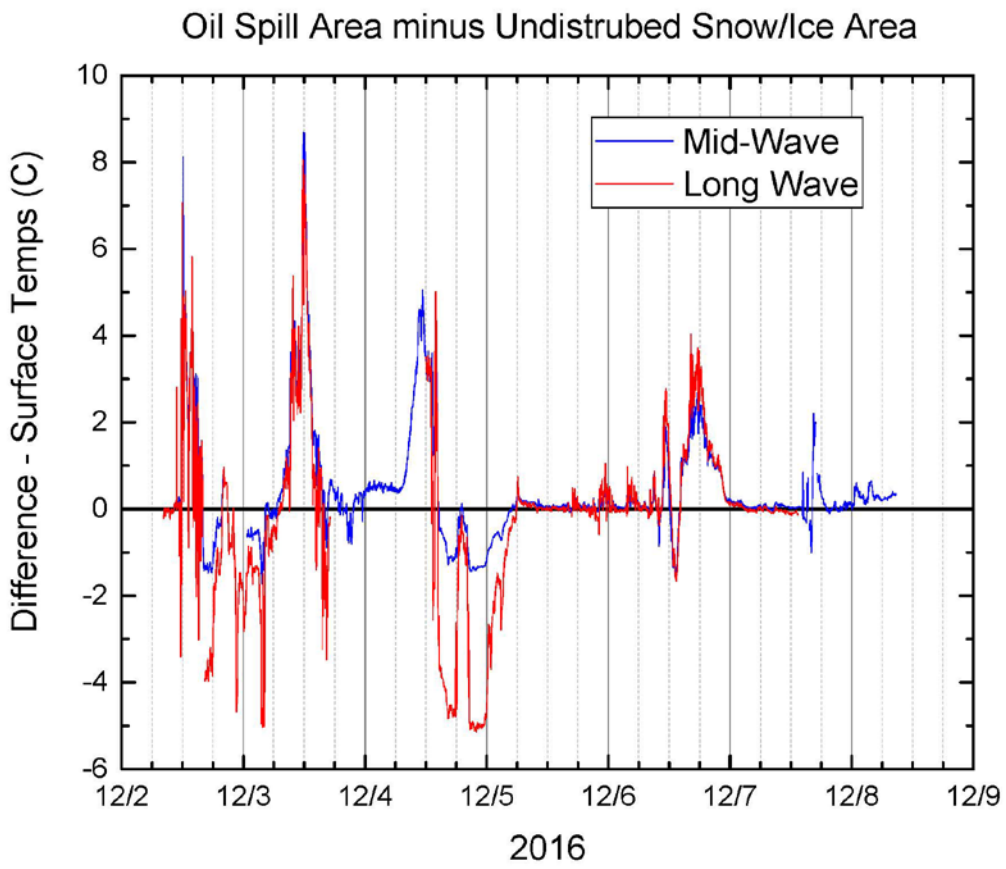

Figure 8 Comparison of long wave and mid wave differences in areas of interest.

5 CONCLUSIONS

These experiments were performed in early December a few weeks before the winter equinox. This represents a worst-case test of IR sensors because in terms of duration of daylight. Short periods of daylight lead to less solar loading of the oiled and clean ice targets under investigation. In contrast, most oil and gas exploration scenarios that could result in an oil on ice event will take place during the Arctic summer with almost unlimited daylight. Even in the worst case scenario represented here, positive detection of oil with both long-wave and mid-wave sensors under low incidence angle conditions occurred. This result is encouraging when considering the future role of IR sensors in operational Arctic spill response.

The FLIR pod is a multifaceted tool with the additional benefit of coupling four cameras into one system. In the case where the low light visible camera is compromised, such as in fog or rain, the user can switch to an alternative, on-board system. The contrast between oil and ice is possible under the correct solar loading conditions. The low light visible spectrum camera is capable of identifying surface oil spills under ideal weather conditions. At present, oil detection is completely dependent on the ability of the operator to visually interpret the image. However, an instrumented long wave, mid wave, or combination infrared sensor system could potentially use an automated process to detect a surface oil spill. In that case, data recorded from infrared sensors could be compared and processed to output an audio or visual alert distinguishing detect from non-detect.

For a period of a few hours after sunset, the oil could become colder than the surrounding snow or ice due to the temperature reversal effect of efficient black body radiation. This effect could further extend the window of operation for IR sensors beyond the daylight period.

Over the next few decades, oil and gas exploration will likely take place in the summer mostly open water period. A loss of well control incident late in the season might result in oil being deposited beneath newly forming ice. This oil would then appear on the ice surface the following spring with close to 24 hours daylight. Based on the results of this study such a scenario would represent an ideal case for IR detection.

ACKNOWLEDGMENTS

We gratefully acknowledge funding of this work through the Arctic Oil Spill Response Technology Joint Industry Programme (JIP). We thank M. Winkler, B. Parker and B. Martin (Shell) for coordinating the use of the FLIR multi-camera pod. We also thank W. Burch and C. Schelewa (CRREL) for their ingenuity and dedication with the technical support of this effort. We would also like to express our gratitude to J. Crary, M. Sadonsky, and J. Adams (CRREL) for their expertise and guidance on refrigeration of the GRF during the fall season when the operation of outdoor cold facilities are nontrivial.

REFERENCES

[1] Transportation Research Board and National Research Council. 2014. Responding to Oil Spills in the U.S. Arctic Marine Environment. The National Academies Press, Washington D.C.

[2] SL Ross Environmental Research, DF Dickins Associates and Envision Planning. 2010. Beaufort Sea oil Spills State of knowledge Review and Identification of Key Issues. Report prepared for Environmental Studies Research Funds (ESRF), Calgary, AB, Canada.

[3] Norcor Engineering. 1975. The Interaction of Crude Oil with Arctic Sea Ice. Beaufort Sea Technical Report 27, Beaufort Sea Project, Department of the Environment, Victoria, B.C., Canada.

[4] M. Fingas, and C. Brown. 2014. Review of Oil Spill Remote Sensing. Marine Pollution Bulletin vol 83.